

# Realizing chiral quantum walks

Dawei Lu,<sup>1</sup> Jacob D. Biamonte,<sup>2</sup> Jun Li,<sup>1</sup> Hang Li,<sup>1</sup> Tomi H. Johnson,<sup>3,4,5,2</sup> Ville Bergholm,<sup>2</sup> Mauro Faccin,<sup>2</sup> Zoltán Zimborás,<sup>6,7</sup> Raymond Laflamme,<sup>1,8</sup> Jonathan Baugh,<sup>1,9,\*</sup> and Seth Lloyd<sup>10,2</sup>

<sup>1</sup>*Institute for Quantum Computing and Department of Physics,  
University of Waterloo, Waterloo N2L 3G1, Ontario, Canada*

<sup>2</sup>*ISI Foundation, Via Alassio 11/c, 10126 Torino, Italy*

<sup>3</sup>*Centre for Quantum Technologies, National University of Singapore, 3 Science Drive 2, 117543, Singapore*

<sup>4</sup>*Keble College, University of Oxford, Parks Road, Oxford OX1 3PG, United Kingdom*

<sup>5</sup>*Clarendon Laboratory, University of Oxford, Parks Road, Oxford OX1 3PU, United Kingdom*

<sup>6</sup>*Department of Computer Science, University College London, Gower St, London WC1E 6BT, UK*

<sup>7</sup>*Department of Theoretical Physics, University of the Basque Country UPV/EHU, 48080 Bilbao, Spain*

<sup>8</sup>*Perimeter Institute for Theoretical Physics, Waterloo, Ontario, Canada*

<sup>9</sup>*Department of Chemistry, University of Waterloo, Waterloo N2L 3G1, Ontario, Canada*

<sup>10</sup>*Massachusetts Institute of Technology, Department of Mechanical Engineering, Cambridge MA 02139 USA*

Given its importance to many other areas of physics, from condensed matter physics to thermodynamics, time-reversal symmetry has had relatively little influence on quantum information science. Here we develop a network-based picture of time-reversal theory, classifying Hamiltonians and quantum circuits as time-symmetric or not in terms of the elements and geometries of their underlying networks. Many of the typical circuits of quantum information science are found to exhibit time-asymmetry. Moreover, we show that time-asymmetry in circuits can be controlled using local gates only, and can simulate time-asymmetry in Hamiltonian evolution. We experimentally implement a fundamental example in which controlled time-reversal asymmetry in a circuit leads to near-perfect transport. Our results pave the way for using time-symmetry breaking to control coherent transport, and imply that time-asymmetry represents an omnipresent yet poorly understood effect in quantum information science.

PACS numbers: 03.65.Fd, 03.65.Ca, 03.65.Aa

## 1. INTRODUCTION

Controlling probability transfer in quantum systems is a central challenge faced in several emerging quantum technologies [1–5]. Here we develop an approach based on a complex network theory viewpoint of quantum systems [6–9], in which probability transfer is directed by the controlled breaking of time-reversal symmetry, creating a so-called *chiral quantum walk* [10–14].

The practical importance of time-reversal symmetry breaking stems from the fact that it is equivalent to introducing biased probability flow into a quantum system. It thus enables directed state transfer without requiring a biased (or non-local) distribution in the initial states, or coupling to an environment [10, 15–17].

This work establishes, in terms of the geometry and edge-weights (or gates) of the underlying graph, conditions on what makes a Hamiltonian (or circuit) time-asymmetric. As well as allowing us to classify the time-symmetry of well-known Hamiltonians and circuits, this knowledge allows us to develop active methods to break time symmetry and bias probability transfer, including using circuits to simulate time-symmetry breaking Hamiltonians.

As a demonstration, the most basic time-asymmetric process is identified and realized experimentally using room-temperature liquid state nuclear magnetic resonance (NMR) on a 3-qubit system. We show that time-asymmetry and thus biased probability transport can be controlled with limited access to the system, namely by using local  $z$ -rotations paired with a naturally occurring (or in our case, emulated) time-symmetric evolution. Through symmetry-breaking we achieve state transfer probabilities approaching unity.

Since their recent introduction [10], continuous time chiral quantum walks have been studied in the context of energy transport in ultracold atoms and molecules [11], in non-equilibrium physics [12, 13], and as a method to achieve near perfect state transfer [10, 14]. Our theory extends the contemporary analysis of time-asymmetry such that it can now apply to gate sequences—of which the existing theory of time-symmetry becomes a special case—and presents a network classification of the effect. Our experiments illustrate how active time-reversal symmetry breaking can be utilized with existing quantum technologies in the presence of limited control.

## 2. CHIRAL QUANTUM WALKS

Consider a unitary propagator  $U$  acting on a state space in which we have a preferred basis  $\{|i\rangle\}$ . We view  $U$

---

\* baugh@uwaterloo.ca


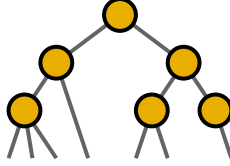
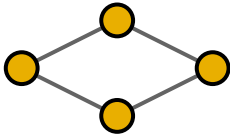
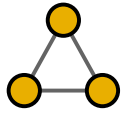
	linear chains	trees (possibly with self-edges)	bipartite graphs (only even cycles)	non-bipartite graphs (some odd cycles)
				
Probability time symmetric ( $\forall \alpha_{ij}$ )?	YES	YES	YES	No
Probability depends on $\alpha_{ij}$ ?	No	No	YES	YES

Table I. In which network geometries do transition probabilities depend on the complex phases  $\alpha_{ij}$  of the edges of the (effective Hamiltonian's) internode coupling graph? We are interested in how the transition probabilities in the site basis depend on  $\alpha_{ij}$  and if certain values of the  $\alpha_{ij}$  can break time-reversal symmetry.

as performing a quantum walk over nodes labeled by  $i$ , and  $U^\dagger$  as performing the time-reversed walk. There are two ways in which the walk  $U$  could be time-symmetric.

*Amplitude time-reversal symmetry* establishes a relationship  $\langle i|U|j\rangle = U_{ij} = (U^\dagger)_{ij}^*$  between the inter-node transition amplitudes going forward and backward in time (where  $*$  denotes complex conjugation and  $^\dagger$  Hermitian conjugation). Equivalently, it establishes a relationship  $U_{ij} = U_{ji}$  between opposing transition amplitudes in the same time direction.

It further implies what we call *probability time-reversal symmetry* (PTS): symmetry of the inter-node transition probabilities going forward and backward in time,  $|U_{ij}|^2 = |(U^\dagger)_{ij}|^2$ . This is equivalent to a lack of directional bias in the transport between any pair of nodes in the same time direction:  $|U_{ij}|^2 = |U_{ji}|^2$ .

Breaking amplitude time-reversal symmetry is a necessary, but not sufficient, condition for breaking probability time-reversal symmetry. In studying internode transport, PTS is the relevant feature. It leads to a richer classification of processes and is the focus of this work.

### 3. HAMILTONIAN EVOLUTIONS

We first consider a unitary propagator  $U = e^{-iHt}$  generated by some time-independent Hamiltonian  $H$ . In our network-based picture, with nodes labeled by  $i$ , we view the matrix elements  $\langle i|H|j\rangle = H_{ij} = h_{ij}e^{i\alpha_{ij}}$  representing Hamiltonian  $H$  as forming a complex adjacency matrix. Here  $h_{ij}$  and  $\alpha_{ij}$  take only real values. For a non-zero value  $H_{ij}$ , two nodes  $i$  and  $j$  are said to be connected by an edge  $e = (i, j)$ , and the complex edge-weight is given by the value of  $H_{ij}$ . A special case is an edge that connects  $i$  to itself, called a self-edge. Since it represents

the expectation value of the energy in state  $|i\rangle$ , the weight  $H_{ii}$  of a self-edge must take a real value. Furthermore, self-edges are only needed if states  $|i\rangle$  have different energies  $H_{ii}$ , otherwise they may be omitted without changing the underlying physics. Taken together, the nodes and edges define a graph, corresponding to the Hamiltonian  $H$ , that we will use to classify the time-symmetry of  $U$ .

We begin by noting that if  $\alpha_{ij} = 0$ , i.e. all edge-weights are real, then both amplitude and probability time-reversal symmetry hold. We now search for other probability time-symmetric Hamiltonians.

A large class of such Hamiltonians are obtained by considering mapping  $H \mapsto \Lambda^\dagger H \Lambda = H'$  (or equivalently  $U \mapsto \Lambda^\dagger U \Lambda = U'$ ), where  $\Lambda$  is a diagonal unitary. Such a mapping will in general affect amplitude time-symmetry. However, it cannot affect transition probabilities as  $|U'_{ij}|^2 = |\langle i|e^{-i\Lambda^\dagger H \Lambda t}|j\rangle|^2 = |\langle i|\Lambda^\dagger e^{-iHt}\Lambda|j\rangle|^2 = |U_{ij}|^2$ , and hence cannot affect probability time-asymmetry. This is why we call these mappings *quasi-gauge symmetry transformations*.

All Hamiltonians that are obtained from a Hamiltonian with real edge-weights by such gauge transformations are thus probability time-symmetric. To give an example, if the graph underlying  $H$  is a tree (of which a linear chain is a special case), there always exists [10] a  $\Lambda$  which removes all phases from the edge-weights:  $H_{ij} = h_{ij}e^{i\alpha_{ij}} \mapsto h_{ij}$ . Such Hamiltonians hence never break probability time symmetry. This gives us our first class of time-symmetric evolutions: those generated by Hamiltonians whose internode couplings form a tree structure (this may include self-edges).

The class of probability time-symmetric networks is richer than those obtained by gauge transformations from real Hamiltonians. To find the other members of this

class, we must consider the interference between walks along different paths. We start by breaking the evolution into commuting even and odd functions of  $H$ :  $U = e^{-iHt} = \cosh(iHt) - \sinh(iHt)$ . The probability time-symmetry condition  $|U_{ij}|^2 = |U_{ji}|^2$  can now be expressed as

$$\sinh(iHt)_{ji} \cosh(iHt)_{ij} = \sinh(iHt)_{ij} \cosh(iHt)_{ji}. \quad (1)$$

The physical interpretation of Eq. (1) is clear:  $\sinh(iHt)_{ij}$  corresponds to transitions along paths of odd length, and  $\cosh(iHt)_{ij}$  to transitions along paths of even length. Together these terms account for all possible paths between  $i$  and  $j$  [18]. A path from  $i$  to itself is called a cycle.

For graph geometries where between each pair of nodes  $(i, j)$  there are only exclusively even or exclusively odd paths (equivalent to there being no odd-length cycles in the graph), probability time-symmetry must always hold as Eq. (1) is always satisfied. Such graphs are called bipartite, where the nodes can be partitioned to two disjoint sets and non-zero edge-weights  $H_{ij} \neq 0$  only connect nodes of different sets [19]. Note that this disallows self-edges, since such edges could be used to make cycles of arbitrary length. Bipartite graphs can also be understood in terms of gauge transformations, as their structure implies the existence of a gauge transformation  $H \mapsto \Lambda^\dagger H \Lambda = -H$ , which immediately implies the probability time-symmetry condition  $|U_{ij}|^2 = |(U^\dagger)_{ij}|^2$ .

This leaves us with two overlapping classes of time-symmetric network geometries, trees with self-edges and bipartite graphs, where the overlap is the class of trees without self-edges or, equivalently, bipartite graphs without simple cycles. The remaining graph geometries are all potentially time-asymmetric, with the degree of asymmetry determined by the values assigned to the edge-weights. These findings are summarized with examples in Table I.

#### 4. QUANTUM CIRCUITS

Consider now instead a unitary propagator  $U$  formed by a palindromic circuit consisting of two-site gates,  $U = \prod_k^{\rightarrow} U_k \prod_k^{\leftarrow} U_k$ . Here the arrows indicate that the second part of the circuit is the reverse of the first, ensuring the circuit is palindromic, since non-palindromic sequences trivially break time-symmetry and thus do not support control over time-symmetry breaking. Each circuit is associated with its support graph, which has an edge if and only if there is a gate in the circuit directly connecting the two sites.

In accordance with the majority of physical implementations, each gate  $U_k = \exp(-iH_k t_k)$  with  $H_k = \sum_{ij \in e_k} (H_k)_{ij} |i\rangle\langle j|$  acts on two sites connected by the edge  $e_k$ . Like before, we explicitly break apart the two complex off-diagonal elements of each gate Hamiltonian, writing  $(H_k)_{ij} = h_k \exp(i\alpha_k) = (H_k)_{ji}^*$ , where  $e_k = (i, j)$ .

We now identify time-symmetric circuits as we did for Hamiltonians.

Our starting point is the case in which each gate is amplitude time-symmetric,  $(U_k)_{ij} = (U_k)_{ji}$ , or equivalently  $\alpha_k = 0$ . This ensures amplitude time-symmetry of the whole palindromic sequence  $U_{ij} = U_{ji}$ , and thus also probability time-symmetry [20]. Once again, we find other time-symmetric circuits by considering gauge transformations  $U \mapsto \Lambda^\dagger U \Lambda$  away from this class of circuits.

Analogous to tree Hamiltonians discussed in the previous section, consider minimal spanning tree circuits, those with only one gate per edge of a tree-like support graph. There is always a gauge transformation that makes every gate amplitude time-symmetric,  $\alpha_k \mapsto 0$ , thus implying that  $U$  must itself be probability time-symmetric.

Likewise, analogous to bipartite Hamiltonians, any circuit with a bipartite support graph with vanishing diagonal Hamiltonian terms  $(H_k)_{ii} = 0$  is gauge equivalent to its inverse, and thus naturally exhibits PTS.

The connection between time-reversal symmetry in circuits and in Hamiltonian evolution can be made even stronger: any Hamiltonian evolution can be simulated by a palindromic circuit of the second-order Trotter type. For simplicity, consider the Hamiltonian evolution  $\exp(-iHt)$  with  $H = \sum_{e \in E} H_e$ , where  $H_e = h \sum_{(i,j)=e} \exp(i\alpha_e) |i\rangle\langle j| + \text{h.c.}$ , for some directed edge-set  $E$ . We construct a palindromic circuit  $U$ , which for each edge  $e \in E$  has a single two-site gate  $U_e = \exp(-iH_e t/2)$ . For small enough values of time-parameter  $\theta = ht$ , the circuit  $U \approx e^{-iHt}$  simulates evolution according to  $H$ . Thus palindromic circuits, our focus, naturally include in them the properties of Hamiltonian evolutions.

We consider a simple implementation of the above Trotter-type circuit using a qubit for each node and working in the single-excitation subspace. Explicitly,  $|j\rangle$  is the state with all qubits in the state  $|0\rangle$ , except  $j$ , which is in the state  $|1\rangle$ . The two-site off-diagonal gates are now two-qubit gates

$$U^{[ij]}(\alpha, \theta) = \exp\left(-i\left[\cos(\alpha)S^{[ij]} + \sin(\alpha)A^{[ij]}\right]\theta/2\right), \quad (2)$$

and are generated by combinations of excitation-number-preserving time-symmetric  $S^{[ij]} = X^{[i]}X^{[j]} + Y^{[i]}Y^{[j]}$  and anti-symmetric  $A^{[ij]} = X^{[i]}Y^{[j]} - Y^{[i]}X^{[j]}$  Hamiltonians, where  $X^{[i]}$ ,  $Y^{[i]}$  and  $Z^{[i]}$  are Pauli matrices acting on qubit  $i$ .

Many systems naturally possess Hamiltonian terms like  $S^{[ij]}$ . Crucially, it is possible to decompose the two-site gate

$$U^{[ij]}(\alpha, \theta) = \mathcal{R}_z^{[j]}(\alpha) U^{[ij]}(0, \theta) \mathcal{R}_z^{[j]\dagger}(\alpha), \quad (3)$$

into a symmetric gate generated by  $S^{[ij]}$  alone, and local  $z$ -rotations  $\mathcal{R}_z^{[j]}(\alpha) = e^{-i(\alpha/2)Z^{[j]}}$  controlling time-asymmetry. Since the  $z$ -rotations can often be placed in

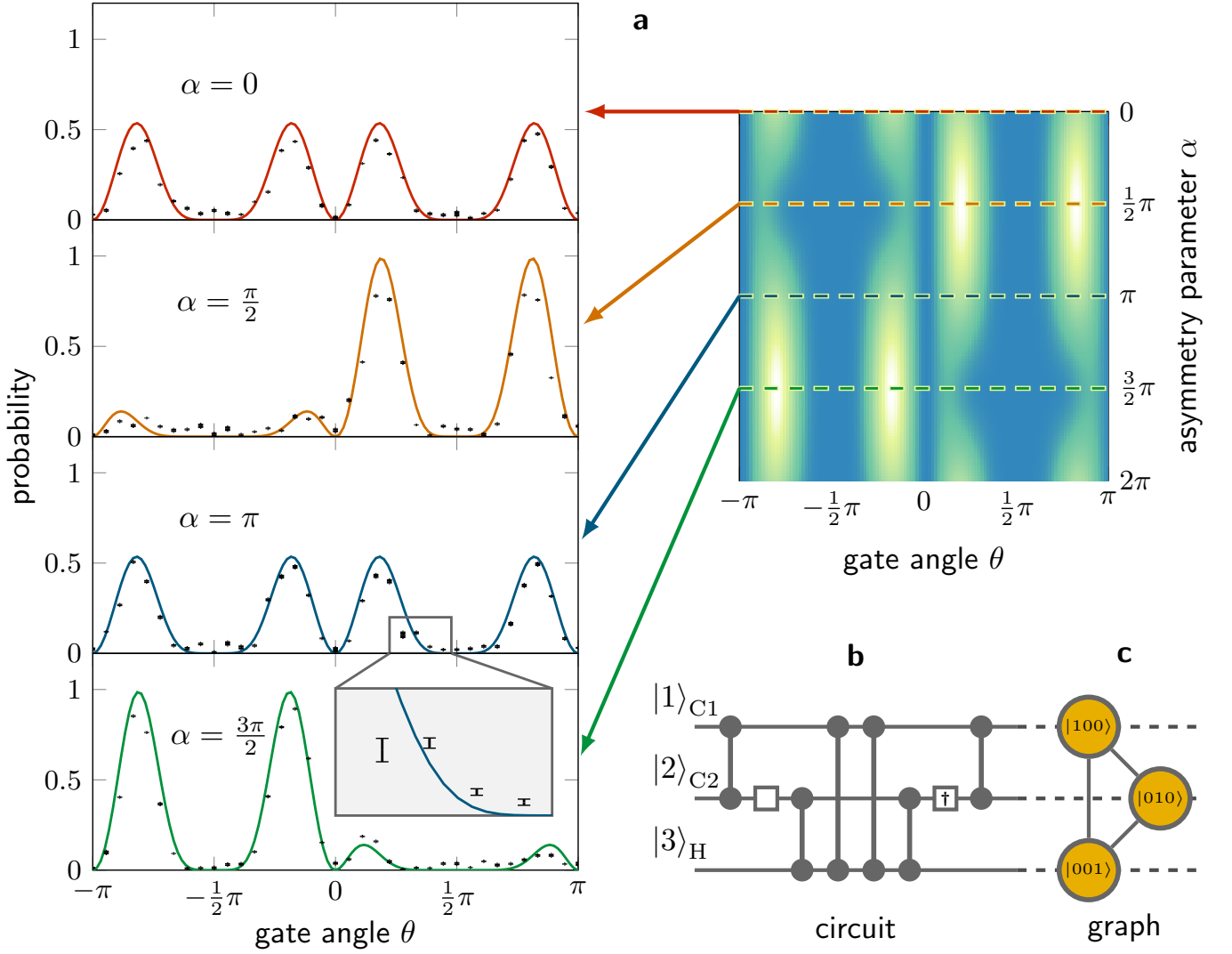


Figure 1. **(a)** The upper right corner depicts the theoretical state-transfer probability  $|\langle 3|U(\alpha, \theta)|1\rangle|^2$ , lighter color indicating higher probability. On the left we present four constant- $\alpha$  slices of this function. Solid lines are theoretical predictions, dots represent experimental data. Dot height represents the experimental error (the inset in the bottom plot highlights the error bars for a few data points). The discrepancies between the theoretical and experimental results are explained by imperfect radiofrequency control fields and decoherence. The rest of the experimental results and a detailed discussion of error sources can be found in section 5. **(b)** Quantum circuit diagram corresponding to the experiment. All the two-qubit gates are of the form  $U^{[ij]}(0, \theta)$  defined in Eq. (2). The left (empty) box in the circuit represents the  $\mathcal{R}_z(\alpha)$  gate and the right box (with dagger  $\dagger$ ) its inverse. **(c)** Graph corresponding to the continuous-time quantum walk (on the single-excitation subspace) simulated by the circuit.

such a way that they combine, often very few rotations are needed to implement  $U$ . For example, controlling the probability time-asymmetry in a ring of  $2N + 1$  spins requires  $2(2N + 1)$  symmetric two-site gates but only 1 pair of  $z$ -rotations.

We will now demonstrate how state transfer can be directed by time-symmetry breaking. The simplest circuit that allows time-symmetry breaking is

$$U(3\alpha, \theta) = U^{[12]}U^{[23]}U^{[31]}U^{[31]}U^{[23]}U^{[12]}, \quad (4)$$

involving three nodes, where all the two-site gates have the same parameters:  $U^{[ij]}(\alpha, \theta)$ . For small enough

gate angles  $\theta = ht$  it simulates the evolution  $U = e^{-iHt}$  according to the most fundamental Hamiltonian  $H = he^{i\alpha}(|1\rangle\langle 2| + |2\rangle\langle 3| + |3\rangle\langle 1|) + \text{h.c.}$  that allows time-symmetry breaking (see Fig. 1c), but we need not be constrained to the regime of small  $\theta$ .

## 5. EXPERIMENT

We implement the circuit in Eq. (4) using NMR techniques in a three-qubit system consisting of  $^{13}\text{C}$ -labeled trichloroethylene dissolved in deuterated chlo-

roform. The implementation requires six symmetric two-site gates and a pair of  $z$ -rotations, shown in Fig. 1b. We directly measure the transition probabilities  $|\langle i|U(\alpha, \theta)|j\rangle|^2$ , while varying both the gate angle  $-\pi < \theta \leq \pi$  and the time-asymmetry parameter  $0 \leq \alpha < 2\pi$ , where time-symmetry occurs only for  $\alpha = n\pi$ .

We display our experimental results for the transport probability from site 1 to site 3 for four values of  $\alpha$  and  $\theta = n\pi/18$  in Fig. 1a. The slice  $\alpha = 0$  corresponds to the amplitude and probability time-symmetric case. The slice  $\alpha = \pi/2$  corresponds to maximum probability time-asymmetry. The slices corresponding to  $\alpha = \pi$  and  $\alpha = 3\pi/2$  represent a reflection in time  $\theta$  of the first two cases.

For the time-symmetric case ( $\alpha = 0$ ) the probabilities of transporting the excitation to the other two spins are always bounded from above by 0.6. However, time-asymmetry ( $\alpha \neq 0$ ) allows us to break this barrier, with transition probabilities approaching unity at the point of maximal time-asymmetry ( $\alpha = \pi/2$ ), as shown in Fig. 1a.

For completeness, we also investigated the cases with the initial excitation localized at spins 2 and 3. The full results are presented in Fig. 3 — illustrating similar properties of time-symmetry breaking and suppression or enhancement of transport probabilities.

The average error of the experimental data relative to the theoretical predictions is about 6.0%, and it can be attributed to two main factors: decoherence and imperfection of GRAPE pulses. The decoherence mainly originates from  $T_2$  relaxation, which induces about 1.5% signal loss. The remaining 4.5% error mostly comes from the imperfection of GRAPE pulses, as well as a minor inhomogeneity of static and radio-frequency magnetic fields.

### Experimental setup

All experiments are carried out on a Bruker DRX 700 MHz NMR spectrometer at room temperature. The sample is  $^{13}\text{C}$ -labeled trichloroethylene (TCE) dissolved in deuterated chloroform. The structure of the molecule is shown in Fig. 2a, where we denote C1 as qubit 1, C2 as qubit 2, and H as qubit 3. The natural Hamiltonian of this system is

$$H = \sum_{j=1}^3 \pi \nu_j Z^{[j]} + \frac{\pi}{2} (J_{13} Z^{[1]} Z^{[3]} + J_{23} Z^{[2]} Z^{[3]}) + \frac{\pi}{2} J_{12} (X^{[1]} X^{[2]} + Y^{[1]} Y^{[2]} + Z^{[1]} Z^{[2]}), \quad (5)$$

where  $\nu_j$  is the chemical shift of the  $j$ th spin and  $J_{ij}$  is the scalar coupling strength between spins  $i$  and  $j$ . As the difference in the chemical shifts between C1 and C2 is not large enough to adopt the weak  $J$ -coupling approximation [21], these two carbon spins are treated as strongly coupled. The parameters of the Hamiltonian are

determined by iteratively fitting the simulated and experimental spectra, and presented in the table in Fig. 2b.

Without loss of generality, we will describe the experimental procedure with spin 1 initially excited, i.e.,  $|100\rangle$  as the initial state. Each experiment consists of three main parts: (A) State initialization: Preparing the system in the pseudo-pure state  $|000\rangle$ , and then exciting one spin to the state  $|100\rangle$ ; (B) Evolution: Driving the system through a palindromic quantum circuit; (C) Measurement: Measuring the probabilities of finding the excitation at each of the spins.

(A) *State initialization.* Starting from thermal equilibrium, we first create the pseudo-pure state

$$\rho_{000} = (1 - \epsilon)\mathbb{1}/8 + \epsilon|000\rangle\langle 000|, \quad (6)$$

using the spatial averaging technique [22]. Here  $\epsilon \approx 10^{-5}$  quantifies the polarization of the system and  $\mathbb{1}$  is the  $8 \times 8$  identity matrix. Next, we apply a  $\pi$  pulse on spin 1 to rotate it to the excited state  $|1\rangle$ . This  $\pi$  rotation is realized by a 2 ms and over 99.5% simulated fidelity Gradient Ascent Pulse Engineering (GRAPE) pulse [23, 24]. All GRAPE pulses in the experiment are designed to be robust against the inhomogeneity of radio-frequency pulses.

(B) *Evolution.* The initial state will be evolved under four types of effective Hamiltonians: a symmetric Hamiltonian  $S^{[ij]}$  and its time reversed version  $-S^{[ij]}$ , and the asymmetric Hamiltonian  $A^{[ij]}$  and its time reversed version, all obtained from  $S^{[ij]}$  using local  $\mathcal{R}_z$  pulses as shown in Eq. (3). The circuit of the entire sequence is depicted in Fig. 1b, where the six two-body interactions form an palindromic circuit for this 3-qubit system. (Note that the two central gates can be merged into a single gate, corresponding to a five-gate palindrome.) We further note that the gate from Eq. (3) can be expressed analytically as

$$\begin{aligned} U^{[ij]}(\alpha, \theta) &= \mathcal{R}_z^{[j]}(\alpha) U^{[ij]}(0, \theta) \mathcal{R}_z^{[j]\dagger}(\alpha) \\ &= \frac{1}{2} (1 + Z^{[i]} Z^{[j]} + \cos(\theta)(1 - Z^{[i]} Z^{[j]}) \\ &\quad - i \sin(\theta) (\cos(\alpha) S^{[ij]} + \sin(\alpha) A^{[ij]})). \end{aligned} \quad (7)$$

The experiment utilized GRAPE pulses with different lengths to implement all of the two-body interactions, depending on the  $J$ -coupling strength (see the table of Fig. 2b) of the related two spins. The three typical lengths of GRAPE pulses for implementing the two-body interactions are 3 ms for  $J_{12}$ , 2 ms for  $J_{23}$  and 8 ms for  $J_{13}$ , respectively. Therefore, the overall run-time of the circuit comprised of all six evolutions is 26 ms, which is much less than the decoherence time as seen in Fig. 2b. For all four of the Hamiltonian types, we implemented the circuit 37 times as  $\theta$  was chosen to realize every  $\pi/18$  step in  $[-\pi, \pi]$ . The total number of GRAPE pulses is 444 and all pulses have simulated fidelities over 99%.

(C) *Measurement.* After implementing the circuit, we measure the probabilities of finding the excitation at each

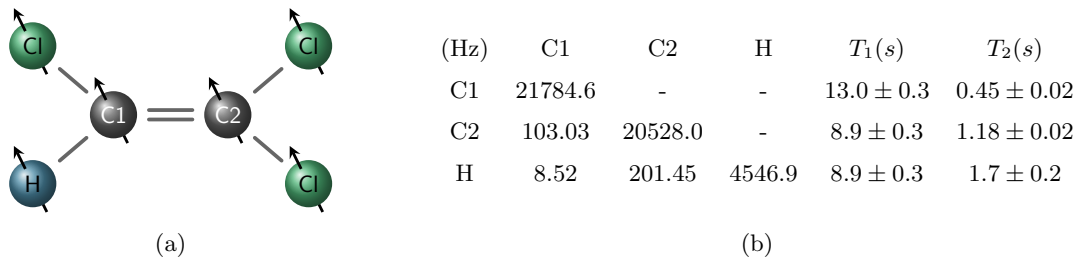


Figure 2. **(a)** Experimental implementation of time-asymmetry controlled transport in NMR using trichloroethylene in which the two  $^{13}\text{C}$  and one  $^1\text{H}$  spins form a 3-qubit register. **(b)** Hamiltonian parameters for the system. The diagonal elements are the chemical shifts  $\nu_i$ , and the off-diagonal elements are scalar coupling strengths  $J_{ij}$ .  $T_1$  and  $T_2$  respectively are the relaxation and dephasing time scales.

spin, i.e. the probabilities of the  $|100\rangle$ ,  $|010\rangle$  and  $|001\rangle$  states, which corresponds to standard population measurement in the NMR setup. We use a  $\pi/2$  pulse to rotate spin 2 to the transverse  $x-y$  plane and compare the relative intensities of the transitions with the initial state. Then all three probabilities can be obtained.

## 6. DISCUSSION

The behavior of the fundamental laws of physics under time-reversal has long remained central to the foundations of physics [25, 26] and has found use in condensed matter theory [27–31]. By going beyond time-independent Hamiltonians to consider quantum circuits and analyze their time-reversal properties, we obtain a far richer set of behaviors. This also provides us a set of new tools for controlling transport in quantum systems.

Focusing on the simplest three-qubit circuit that allows time-symmetry breaking, we experimentally demonstrate that this asymmetry can lead to noticeably enhanced transition probabilities. Further, we show that the circuit’s time-symmetry or lack thereof can be completely controlled by local  $z$ -rotations. This is reminiscent of how one can change the sign of a Hamiltonian by the application of local gates, which is a common tool in NMR experiments [21]. The most elementary example is reversing the sign of a  $\sigma_z$  Hamiltonian with a  $\pi$ -pulse about the  $x$ -axis. A more interesting example is the so-called magic echo for reversing the sign of the homonuclear dipolar

Hamiltonian [32, 33].

We emphasize that time-asymmetric site-to-site transport can only take place in circuits whose circuit graphs have odd cycles (see Table I). We expect our method of directing quantum transport also to be applicable in much larger networks. The amount of enhancement achievable will most likely be heavily dependent on the topology of the network and the structure of the gate sequence, an interesting topic for future research.

## ACKNOWLEDGMENTS

VB, JDB, MF, THJ and ZZ completed parts of this study while visiting the Institute for Quantum Computing at the University of Waterloo, and acknowledge financial support from the Fondazione Compagnia di San Paolo through the Q-ARACNE project. JDB acknowledges the Foundational Questions Institute (FQXi, under grant FQXi-RFP3-1322) for financial support. THJ acknowledges the National Research Foundation and the Ministry of Education of Singapore for funding. ZZ acknowledges support from the EPSRC and by the EU through the ERC Starting Grant GEDENTQOPT and the CHIST-ERA QUASAR project. DL, JL, HL, RL and JB acknowledge Industry Canada, NSERC and CIFAR for financial support. SL acknowledges the ARO, DARPA, AFOSR, Eni via MITEI, and Jeffrey Epstein for financial support.

- 
- [1] J. A. Jones and M. Mosca, “Implementation of a quantum algorithm on a nuclear magnetic resonance quantum computer,” *J. Chem. Phys.* **109**, 1648–1653 (1998).
  - [2] Lieven M.K. Vandersypen, Matthias Steffen, Gregory Breyta, Costantino S. Yannoni, Mark H. Sherwood, and Isaac L. Chuang, “Experimental realization of Shor’s quantum factoring algorithm using nuclear magnetic resonance,” *Nature* **414**, 883–887 (2001).
  - [3] B. P. Lanyon *et al.*, “Towards quantum chemistry on a quantum computer,” *Nature Chemistry* **2**, 106–111 (2010), arXiv:0905.0887.
  - [4] Jingfu Zhang, Man-Hong Yung, Raymond Laflamme, Alán Aspuru-Guzik, and Jonathan Baugh, “Digital quantum simulation of the statistical mechanics of a frustrated magnet,” *Nat. Commun.* **3**, 880 (2012).
  - [5] Florian Dolde, Ville Bergholm, Ya Wang, *et al.*, “High fidelity spin entanglement using optimal control,” *Nat. Commun.* **5**, 3371 (2014), arXiv:1309.4430.
  - [6] Mauro Faccin, Tomi Johnson, Jacob Biamonte, Sabre Kais, and Piotr Migdał, “Degree distribution in quan-

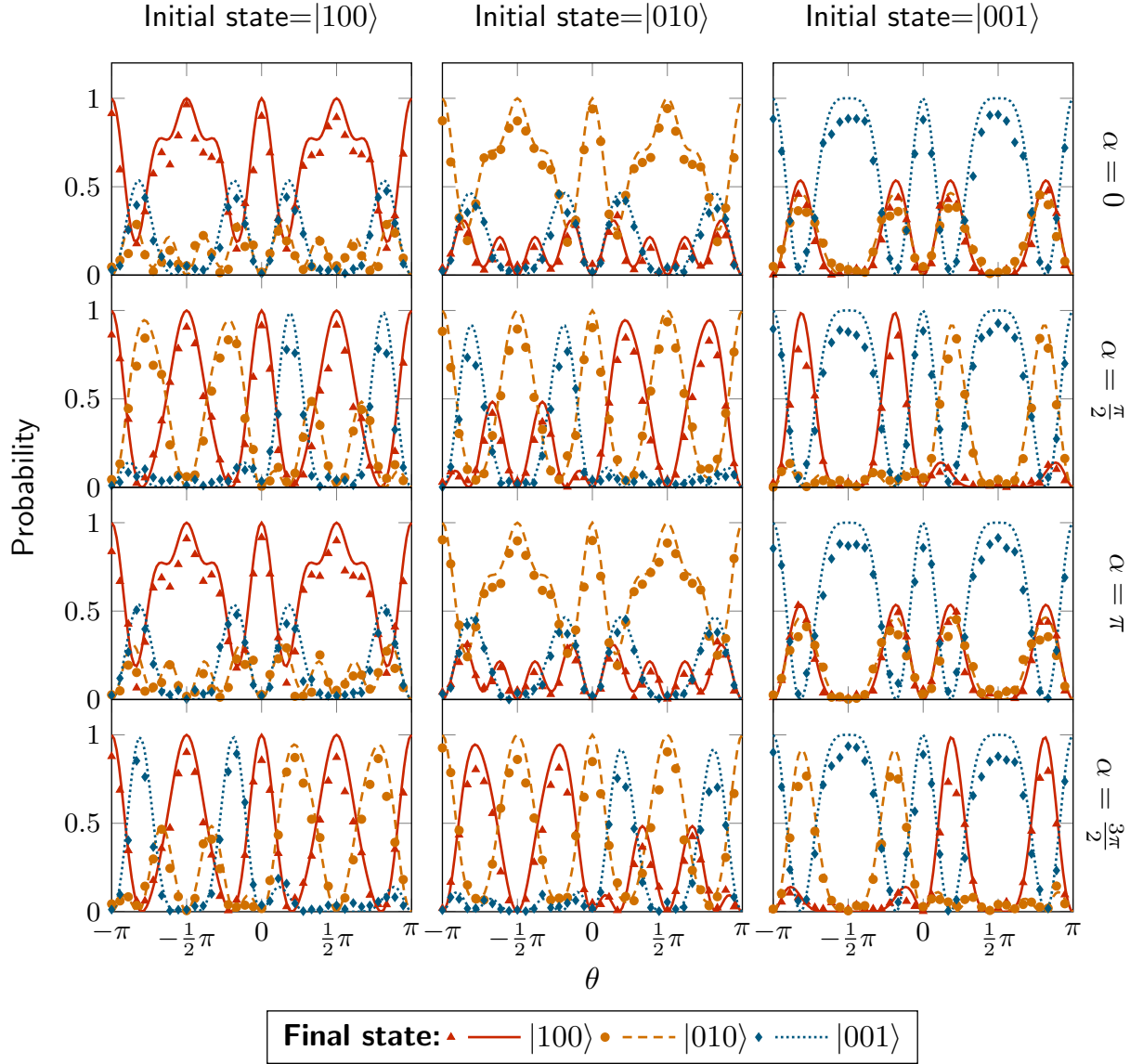


Figure 3. Experimental results of time-asymmetry controlled transport on the 3-qubit NMR system. The three columns correspond to different initial states ( $|100\rangle$ ,  $|010\rangle$  and  $|001\rangle$ ). The red solid, yellow dashed and blue dotted curves are the theoretical probabilities of measuring  $|100\rangle$ ,  $|010\rangle$  and  $|001\rangle$ , respectively. The triangles, circles and diamonds represent the corresponding experimental results. Experimental values are measured at 36 equally spaced ( $\pi/18$ ) time steps in the range from  $-\pi$  to  $\pi$ . The plots with  $\alpha = 0, \pi$  correspond to time-symmetric gates and its time-reversed evolution (which cannot break time symmetry). The plots with  $\alpha = \pi/2, 3\pi/2$  correspond to time-asymmetric gates and its time-reversed evolution, which do exhibit time-reversal asymmetry.

- tum walks on complex networks,” *Phys. Rev. X* **3**, 041007 (2013).
- [7] O. Mülken and A. Blumen, “Continuous-time quantum walks: Models for coherent transport on complex networks,” *Phys. Rep.* **502**, 37–87 (2011).
- [8] Andrew M. Childs, “Universal computation by quantum walk,” *Phys. Rev. Lett.* **102**, 180501 (2009).
- [9] S. Perseguers, M. Lewenstein, A. Acín, and J. I. Cirac, “Quantum random networks,” *Nature Physics* **6**, 539–543 (2010).
- [10] Z. Zimborás, M. Faccin, Z. Kádár, J. D. Whitfield, B. P. Lanyon, and J. Biamonte, “Quantum transport enhancement by time-reversal symmetry breaking,” *Sci. Rep.* **3**, 2361 (2013), arXiv:1208.4049.
- [11] Ping Xiang, Marina Litinskaya, Evgeny A. Shapiro, and Roman V. Krems, “Non-adiabatic control of quantum energy transfer in ordered and disordered arrays,” *New J. Phys.* **15**, 063015 (2013).
- [12] Salil Bedkihal, Malay Bandyopadhyay, and Dvira Segal, “The probe technique far from equilibrium: Magnetic field symmetries of nonlinear transport,” *Eur. Phys. J. B* **86**, 506 (2013).
- [13] Daniel Manzano and Pablo I. Hurtado, “Symmetry and the thermodynamics of currents in open quantum sys-



- tems,” *Phys. Rev. B* **90**, 125138 (2014).
- [14] Stephen Cameron, Shannon Fehrenbach, Leah Granger, Oliver Hennigh, Sunrose Shrestha, and Christino Tamon, “Universal state transfer on graphs,” *Linear Algebra Appl.* **455**, 115–142 (2014).
  - [15] M. B. Plenio and S. F. Huelga, “Dephasing-assisted transport: quantum networks and biomolecules,” *New J. Phys.* **10**, 113019 (2008).
  - [16] I. Sinayskiy, A. Marais, F. Petruccione, and A. Ekert, “Decoherence-assisted transport in a dimer system,” *Phys. Rev. Lett.* **108**, 020602 (2012), arXiv:1401.3298.
  - [17] Sougato Bose, “Quantum communication through spin chain dynamics: an introductory overview,” *Contemporary Physics* **48**, 13–30 (2007).
  - [18] It is not entirely necessary to consider all possible paths between two nodes as *a priori* prescribed by Eq. (1). For a process with  $N$  nodes, the Cayley-Hamilton theorem asserts the existence of a vanishing polynomial with highest degree at most  $N$ . This implies that transitions of higher order can be expressed in terms of  $N$ -long paths.
  - [19] This is seen by considering a connected graph with this property, i.e., any two nodes are connected with paths that have either exclusively of odd or of even lengths. Let  $n$  be an arbitrary node, and denote by  $A$  the set of nodes that are connected to  $n$  with paths of even lengths and by  $B$  the nodes that are connected to  $n$  with paths of odd lengths. The union of  $A$  and  $B$  contain all the nodes, the intersection of  $A$  and  $B$  is empty, and any node in  $A$  is directly connected only to nodes in  $B$  and vice versa; hence the graph is bipartite.
  - [20] An elementary example of a common circuit family that induces amplitude symmetric evolutions is palindromic *reversible circuits*. The analogous case of probability time-reversal symmetry is found by considering self-inverse circuit families: with the prototypical example given by *Clifford gate or stabilizer circuits*.
  - [21] L. M. K. Vandersypen and I. L. Chuang, “NMR techniques for quantum control and computation,” *Rev. Mod. Phys.* **76**, 1037–1069 (2005).
  - [22] David G. Cory, Amr F. Fahmy, and Timothy F. Havel, “Ensemble quantum computing by NMR spectroscopy,” *Proc. Natl. Acad. Sci.* **94**, 1634–1639 (1997).
  - [23] Navin Khaneja, Timo Reiss, Cindie Kehlet, Thomas Schulte-Herbrüggen, and Steffen J. Glaser, “Optimal control of coupled spin dynamics: design of NMR pulse sequences by gradient ascent algorithms,” *J. Magn. Reson.* **172**, 296–305 (2005).
  - [24] C. A. Ryan, C. Negrevergne, M. Laforest, E. Knill, and R. Laflamme, “Liquid-state nuclear magnetic resonance as a testbed for developing quantum control methods,” *Phys. Rev. A* **78**, 012328 (2008).
  - [25] E. P. Wigner, *Group Theory and its Application to the Quantum Mechanics of Atomic Spectra* (New York: Academic Press, 1959).
  - [26] M. Skotiniotis, B. Toloui, I. T. Durham, and B. C. Sanders, “Quantum frameness for cpt symmetry,” *Phys. Rev. Lett.* **111**, 020504 (2013), arXiv:1306.6114.
  - [27] R. Peierls, “On the theory of diamagnetism of conduction electrons,” *Z. Phys.* **80**, 763–791 (1933).
  - [28] Douglas R. Hofstadter, “Energy levels and wave functions of Bloch electrons in rational and irrational magnetic fields,” *Phys. Rev. B* **14**, 2239–2249 (1976).
  - [29] Sankar Das Sarma and Aron Pinczuk, *Perspectives in quantum Hall effects* (John Wiley & Sons, 2008).
  - [30] M. Z. Hasan and C. L. Kane, “Colloquium: Topological insulators,” *Rev. Mod. Phys.* **82**, 3045–3067 (2010).
  - [31] Jean Dalibard, Fabrice Gerbier, Gediminas Juzeliūnas, and Patrik Öhberg, “Colloquium: Artificial gauge potentials for neutral atoms,” *Rev. Mod. Phys.* **83**, 1523–1543 (2011).
  - [32] W-K. Rhim, A. Pines, and J. S. Waugh, “Time-reversal experiments in dipolar-coupled spin systems,” *Phys. Rev. B* **3**, 684–696 (1971).
  - [33] H. Cho, Thaddeus D. Ladd, Jonathan Baugh, David G. Cory, and Chandrasekhar Ramanathan, “Multispin dynamics of the solid-state NMR free induction decay,” *Phys. Rev. B* **72**, 054427 (2005).